Supplementary Information

"Dependence of Single Molecule Junction Conductance on Molecular Conformation"

Latha Venkataraman[1,4], Jennifer E. Klare[2,4], Colin Nuckolls[2,4], Mark S. Hybertsen[3,4], Michael Steigerwald[2]
[1]*Department of Physics,*
[2]*Department of Chemistry,*
[3]*Department of Applied Physics and Applied Mathematics, and*
[4]*Center for Electron Transport in Molecular Nanostructures*
Columbia University, New York, New York

Content:

Experimental Procedures:

We measure the molecular conductance by repeatedly forming and breaking Au point contacts in an environment of molecules with a modified scanning tunneling microscope (STM). The setup and method has been described in detail elsewhere[1, 2]. Briefly, Au point-contacts formed between the STM tip and substrate, were broken in ambient at room temperature in a freshly prepared 1 mM solution of the molecules in 1,2,4-trichlorobenzene (99% Aldrich), trapping one or more molecules between the ends of the broken Au point-contact. The current was recorded at a fixed bias voltage of 25 mV while the electrodes were pulled apart at a rate of 20 nm/s. For all measurements presented, the current to voltage converter gain was set at 10^{-6}A/V. This process was repeated generating of thousands conductance traces without any selection criteria. Typically, conductance traces were collected on more than one tip/substrate pair for each molecule measured. Histograms were constructed from the current versus position traces by converting currents to conductances and binning the data as a function of conductance. All histograms were constructed from all collected traces with no selection whatsoever. For all histograms constructed, the counts were divided by the number of traces used to construct histograms so as to be able to compare histograms constructed from different number of traces for each molecule (the number of traces collected varied between 3000 and 12000 for different molecules). To ensure that each measurement started from a different initial atomic configuration, the electrodes were pulled apart only after being brought into contact with the Au surface, indicated by a conductance greater than a few G_0. For each tip/substrate pair, we constructed conductance histograms with 1000 traces without molecules to ensure that we had a clean substrate.

The molecular junction conductance values were determined from a Lorentzian fit to the histograms with functional form: $f(G) = A/((G-G_{peak})^2+B^2)$. Here, G_{peak} is the peak conductance. The scaled histogram widths (W_{peak}), defined as B/G_{peak}, are determined from the fit to the data. For each molecule measured, the histogram for each set of 1000 traces was individually fit with a Lorentzian to determine G_{peak} and $W_{peak.}$ The molecule conductance and width listed in Table 1 are the mean G_{peak} and W_{peak} values from all the fits for each molecule. The error bars in Figure 2C and Figure 3A are the standard deviation of the G_{peak} values. For most molecules, a Lorentzian fits the peak region and the high conductance tail well, whereas a Gaussian fit to the peak region does not fit the high conductance tail of the histogram. This is because individual traces are not precisely flat, but have a small slope and hence are fit better by a tangent function. When we use a previously detailed algorithm[1] to select traces which have flat steps, the histogram constructed from the selected curves can be fit to a Gaussian function. For molecule **8**, a Lorentzian was fit to the data after subtraction of a gold histogram as the peak was to close to our resolution limit at the gain settings of the current to voltage converter used for all measurements. For molecule **9**, the Lorentzian that fit the high conductance tail of the peak did not fit the region around the peak well hence we used the actual maximum of the peak for the molecule conductance. The difference between the two was within our experimental error for this molecule.

Sample Conductance Traces:

Figure S1: *Sample conductance traces, shown on a semi-log scale, measured in solutions of (a) no molecules, (b) 1,4-diaminobenzene, and (c) 2,7-diaminofluorene.*

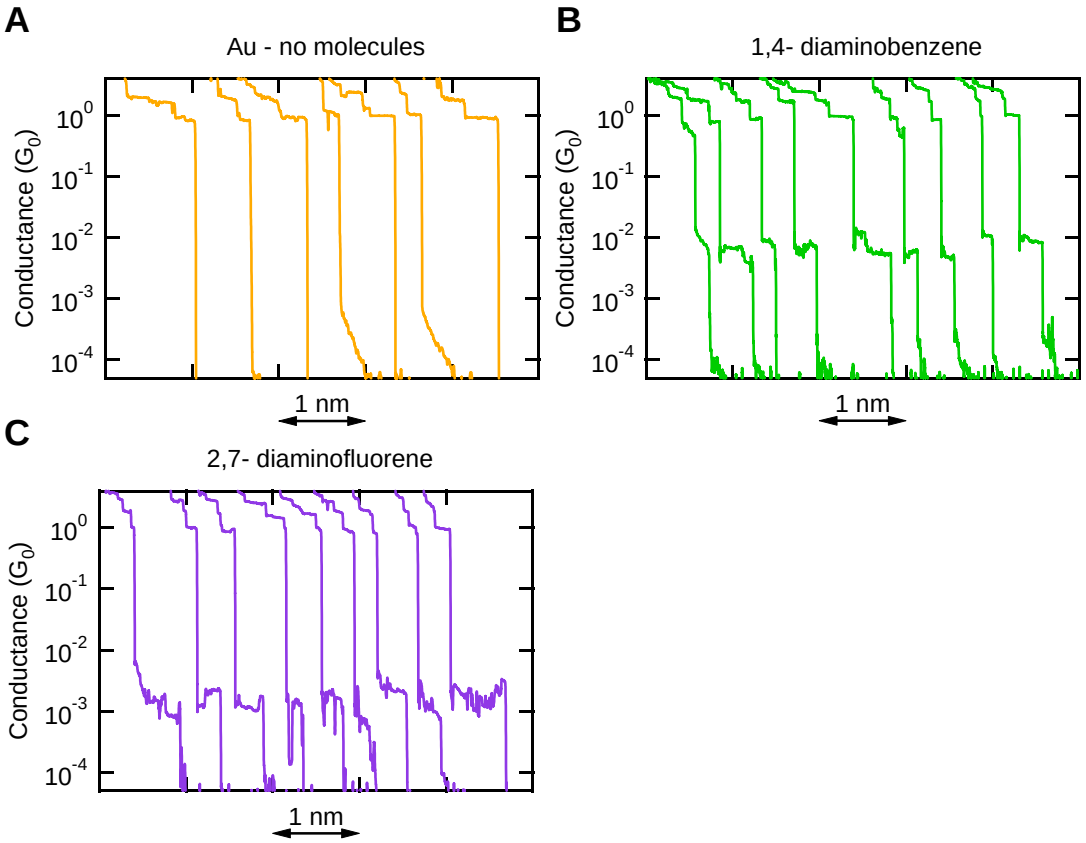

Figure S2: Sample conductance traces, shown on a semi-log scale, measured in solutions of (a) 4,4-diaminobiphenyl and (b) 4,4'-diamino-p-terphenyl.

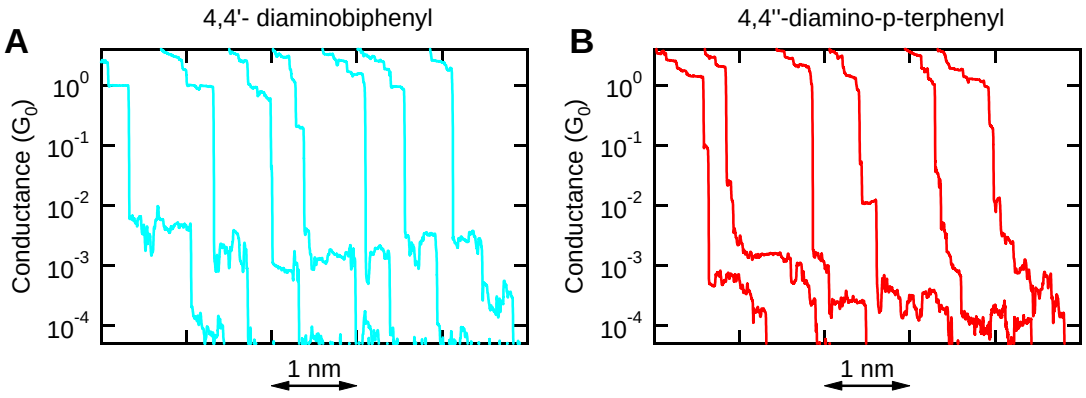

Synthetic Procedures:

General. Starting materials and reagents were obtained from commercial sources or synthesized by procedures noted below. 1,4-diaminobenzene (**1**), 2,7-diaminofluorene (**2**), dihydroethidium (**3**) and 4,4'-diaminobiphenyl (**4**), 4,4'-diaminooctafluorobiphenyl

(**6**) 4,4'diamino 2,5,2',5' tetrachlorobiphenyl (**7**) and 4,4"-diamino-p-terphenyl (**9**) were purchased from Sigma-Aldrich, Alfa Aesar or TCI-America. All commercial molecules were used as purchased (typically 98% purity or higher) except for molecule **6** which was purified prior to use. 2,6,2',6'-tetramethyl 4,4'diaminobiphenyl (**8**) was synthesized following a previously published procedure[3]. 4,4'-diamino-2-methyl-biphenyl (**5**) was synthesized following method detailed below.

Anhydrous and oxygen-free solvents (CH_2Cl_2, Et_2O, THF, and toluene) were obtained from a Schlenk manifold with purification columns packed with activated alumina and supported copper catalyst (Glass Contour, Irvine, CA) [4]. Column chromatography was performed on a CombiFlash Sg100c system using RediSep normal phase silica columns (ISCO, Inc., Lincoln, NE). ^{1}H NMR (300MHz) and ^{13}C NMR (75MHz) were recorded on a Bruker DRX 300. ^{1}H NMR resonances were referenced to the respective solvent peak. Infrared spectra were recorded on a BioRad FTS 7000 FT-IR spectrometer using KBr plates or pellets.

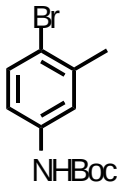

Compound 10. To a round bottom flask with a magnetic stir bar was added 4-Bromo-3-methyl-aniline (Aldrich, 1.00 g, 5.37 mmol) and anhydrous THF (20 mL). At 0^o C, Boc_2O (Aldrich, 1.40 g, 6.44 mmol) was added and the mixture was allowed to warm to room temperature and then refluxed for 12 hrs. The compound was directly loaded onto silica gel, and the product was isolated as a yellow solid (1.22 g, 79%) by silica gel chromatography.

^{1}H NMR (300 MHz, $CDCl_3$) δ 7.40 (d, *J* = 8.6 Hz, 1H), 7.32 (d, *J* = 2.3 Hz, 1H), 7.02 (m, 1H), 6.86 (s, 1H), 2.36 (s, 3H), 1.51 (s, 9H) ppm; ^{13}C NMR (75 MHz, $CDCl_3$) δ 152.7, 138.6, 137.7, 132.7, 120.8, 118.2, 117.6, 80.9, 28.5, 23.2 ppm; FTIR (thin film): 3308, 2985, 1696, 1588, 1533, 1400, 1284, 1156, 1058, 814 cm^{-1}. HRMS (FAB+, [M+]) calcd for $C_{12}H_{16}O_2NBr$ 285.0364 *m/z*; found 285.0370 *m/z*.

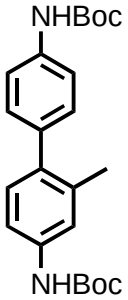

Compound 11. To a round bottom flask with a magnetic stir bar was added **10** (0.437 g, 1.53 mmol), t-butyl N-[4-(4,4,5,5-tetra-methyl-1,3,2-dioxaborolan-2-yl)phenyl]carbamate (Aldrich, 0.30 g, 1.53 mmol), $Pd(PPh_3)_4$ (Strem, 0.176 g, 0.153 mmol), K_2CO_3 (1.70 g, 12.24 mmol), anhydrous THF (20 mL), and degassed water (2 mL). The mixture was

refluxed with stirring for 16 hours. Ether (10 mL) and brine was added and the layers were separated. The ether layer was loaded onto silica gel, and the product was isolated as a white solid (0.235 g, 39%) by silica gel chromatography.
^{1}H NMR (300 MHz, $CDCl_3$) δ 7.38 (d, *J* = 8.5 Hz, 2H), 7.30 (s, 1H), 7.21 (d, *J* = 8.6 Hz, 2H), 7.13 (m, 2H), 6.54 (s, 1H), 6.48 (s, 1H), 2.24 (s, 3H), 1.53 (s, 18H) ppm; ^{13}C NMR (75 MHz, $CDCl_3$) δ 152.98, 137.36, 137.09, 136.45, 130.47, 129.98, 120.40, 118.41, 116.2, 80.69, 80.63, 28.50, 20.79 ppm; FTIR (thin film): 3330, 2979, 2931, 1701, 1589, 1514, 1236, 1161, 1059, 733 cm^{-1}. HRMS (FAB+, [M+]) calcd for $C_{23}H_{30}O_4N_2$ 398.2206 *m/z*; found 398.2217 *m/z*.

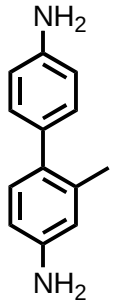

Compound 5. Compound **11** (0.014 g, 13.1 μmol) was dissolved in 3 mL CH_2Cl_2 and 3 mL TFA and stirred at room temperature for two hours. Removal of the solvent and acid *in vacuo* resulted in a white solid (0.113 g, 97%).
^{1}H NMR (300 MHz, DMSO) δ 8.70 (b, 4H), 7.23 (d, *J* = 8.5 Hz, 2H), 7.12 (d, *J* = 7.9 Hz, 1H), 7.04 (d, *J* = 8.4 Hz, 2H), 6.95 (m, 2H), 2.20 (s, 3H) ppm; ^{13}C NMR (75 MHz, DMSO) δ 136.0, 130.5, 1230.0, 121.3, 118.7, 117.4, 20.3 ppm; FTIR (KBr pellet): 3004 (broad), 1672, 1493, 1203, 1136 cm^{-1}. LRMS (APCI+, [M+]) calcd for $C_{13}H_{15}N_2$ 199.12 *m/z*; found 199.23 *m/z*.

Theoretical Procedures

The generalized gradient approximation (GGA) as formulated by Perdew, Burke and Ernzerhof (PBE) was used[5]. The molecular calculations were done with Jaguar v5.0[6] using a 6-31g** basis for the light atoms and a lacvp** basis for Au[7]. The molecular geometry was fully relaxed. Each amine-Au link was modeled using a single Au atom. The amine-Au link is characterized by a N-Au bond length of 2.43-2.46 Å and a Au-N-C bond angle of 121-126 degrees. For 1,4-diaminobenzene, Au binds to the amines in a trans configuration. All of the molecules considered in the experiments were studied in this configuration. The average twist angle at the single C-C sigma bond, shown in Table 1 in the main text, is based on geometrical optimization with the amine end groups. The end groups do affect the average twist angle. Biphenyl, without any substitutions or Amine terminations is computed to have a 39 degree twist angle while 4,4'-diaminobiphenyl has a 34 degree twist angle. Binding of each amine to a single Au atom as a proxy for the under-coordinated Au link site in the junction results in a 29 degree twist angle. The influence of the solution is not included in the calculations, though it is believed to be small.

Binding of an Au atom to each amine results in frontier orbitals that are predominantly of Au-s, N lone pair antibonding character. There is a weak coupling due

to tunneling through the molecular backbone resulting in symmetric and antisymmetric frontier orbitals with a splitting, *2t*, that is a measure of the tunnel coupling[8]. These frontier states derived from the amine-Au link reside roughly in the middle of the HOMO-LUMO gap for the phenyl backbone. The conductance is proportional to t^2 in this regime[9], and a relative conductance can be computed for all molecules by scaling t^2 with the measured conductance of 1,4 diaminobenzene as shown in Table 1 in the main text. For reference, the tunnel splitting for diaminobenzene is calculated to be 0.30 eV. For the oligophenyls series, a decay constant can be determined from the t^2 values as shown in Figure S3A. There is an electronic substituent effect on the tunneling matrix element, in addition to the twist angle. For most of the molecules studied, this is a small effect e.g. about a 4% difference between 4,4'-diaminobiphenyl constrained to be flat and the 2,7-diaminofluorene (at a twist angle of 1.5 degrees). The exception is **3**, which shows a tunnel splitting close to that of **2**, despite a twist angle of about 17 degrees.

The impact of dynamical fluctuations, particularly involving the phenyl ring rotation degree of freedom was explored for several situations. The simplest example is illustrated in Figure S3B, showing the configuration energy versus twist angle between the phenyl rings with no constraint imposed by the amine binding in a junction. The twist angle with minimum energy and the barriers at zero and 90 degrees (1.6 and 2.6 kcal/mol respectively) were all derived from diaminobiphenyl calculations with a 6-311g** basis set using the PBE functional. The energy surface is then fit to two cubic polynomial interpolation functions. A thermal average at room temperature results in an average twist angle about 1.5 degrees greater than the minimum, which is within the accuracy of the calculations. The impact on the conductance is estimated assuming a $cos^2\phi$ dependence on the tunneling matrix element. The thermally averaged conductance corresponds to the coupling through a static molecule with twist angle about 2.5 degrees greater than the minimum.

Figure S3. *Trends in the calculated tunneling coupling. A: exponential fit (—) to t^2 against the number of phenyls in the oligophenyl series (•). B: Illustration of the thermal averaging over the internal twist angle degree of freedom for biphenyldiamine. The configuration energy is described in the text and the tunnel probability proportional to $cos^2\phi$ and a Boltzmann factor.*

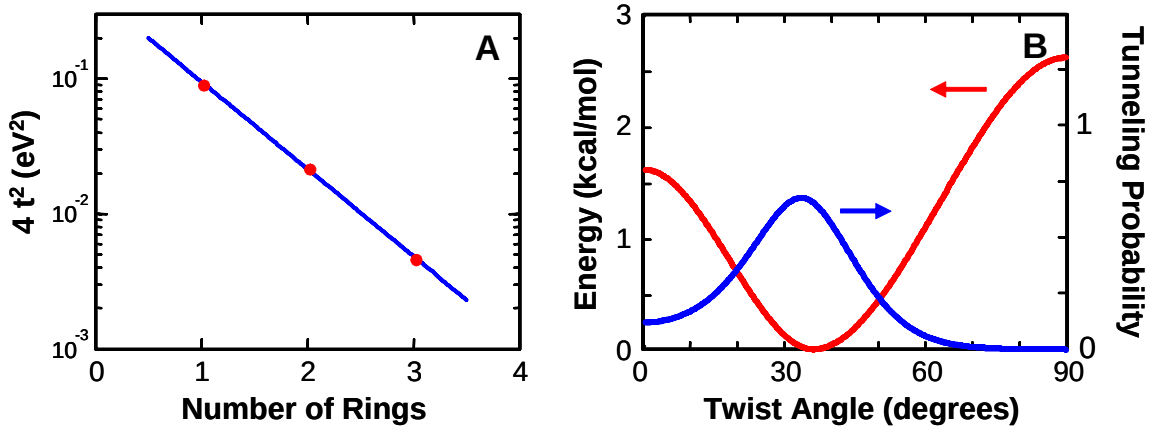

For the molecules with larger average twist angles (molecules **5-7**), the substituents stiffen the potential surface on the small angle side and generally lower the barrier towards the high angle side. As a result, the thermally averaged angles tend to be a few degrees larger and the thermally averaged conductance somewhat lower, corresponding to a static molecule with twist angle 4 to 7 degrees larger than the angle corresponding to the potential minimum.

Careful comparison of the torsional energy surface of biphenyl calculated with DFT (BLYP) and with MP2 using double zeta basis sets[10] suggests some systematic differences. The MP2 calculation gives a larger twist angle at the energy minimum (by 7 degrees) a larger barrier at zero twist (by 2 kcal/mol) and a smaller barrier at 90 degrees (by 1 kcal/mol). However, the impact of thermal averaging remains essentially the same.

In summary, several factors influence our determination of the effective twist angle that controls the average conductance. These include the coupling to the gold, the thermal average and errors intrinsic to the approximations in the DFT calculations. Based on the above discussion, these effects are each a few degrees and to some extent compete. Overall, we believe the angles presented in Table 1, based on static optimization of the amine terminated species, are representative, with an uncertainty of a few degrees due to the other effects.

References:

1. Ulrich, J. et al. Variability of Conductance in Molecular Junctions. Journal of Physical Chemistry B 110, 2462-2466 (2006).
2. Venkataraman, L. et al. Single-Molecule Circuits with Well-Defined Molecular Conductance. Nano Letters 6, 458 - 462 (2006).
3. Helms, A., Heiler, D. & Mclendon, G. Electron-Transfer in Bis-Porphyrin Donor-Acceptor Compounds with Polyphenylene Spacers Shows a Weak Distance Dependence. Journal of the American Chemical Society 114, 6227-6238 (1992).
4. Pangborn, A. B., Giardello, M. A., Grubbs, R. H., Rosen, R. K. & Timmers, F. J. Safe and convenient procedure for solvent purification. Organometallics 15, 1518-1520 (1996).
5. Perdew, J. P., Burke, K. & Ernzerhof, M. Generalized gradient approximation made simple. Physical Review Letters 77, 3865-3868 (1996).
6. Jaguar. (Schrodinger, L.L.C., Portland, OR, 1991-2003).
7. Wadt, W. R. & Hay, P. J. Abinitio Effective Core Potentials for Molecular Calculations - Potentials for Main Group Elements Na to Bi. Journal of Chemical Physics 82, 284-298 (1985).
8. Woitellier, S., Launay, J. P. & Joachim, C. The Possibility of Molecular Switching - Theoretical-Study of [(Nh3)5ru-4,4'-Bipy-Ru(Nh3)5]5+. Chemical Physics 131, 481-488 (1989).
9. Nitzan, A. Electron transmission through molecules and molecular interfaces. Annual Review of Physical Chemistry 52, 681-750 (2001).
10. Karpfen, A., Choi, C. H. & Kertesz, M. Single-bond torsional potentials in conjugated systems: A comparison of ab Initio and density functional results. Journal of Physical Chemistry A 101, 7426-7433 (1997).